

## Effects of dendritic load on the firing frequency of oscillating neurons

Michael A. Schwemmer and Timothy J. Lewis\*

*Department of Mathematics, One Shields Avenue, University of California, Davis, California 95616, USA*

(Received 12 August 2009; revised manuscript received 28 October 2010; published 14 March 2011)

We study the effects of passive dendritic properties on the dynamics of neuronal oscillators. We find that the addition of a passive dendrite can sometimes have counterintuitive effects on firing frequency. Specifically, the addition of a hyperpolarized passive dendritic load can either increase, decrease, or have negligible effects on firing frequency. We use the theory of weak coupling to derive phase equations for “ball-and-stick” model neurons and two-compartment model neurons. We then develop a framework for understanding how the addition of passive dendrites modulates the frequency of neuronal oscillators. We show that the average value of the neuronal oscillator’s phase response curves measures the sensitivity of the neuron’s firing rate to the dendritic load, including whether the addition of the dendrite causes an increase or decrease in firing frequency. We interpret this finding in terms of the slope of the neuronal oscillator’s frequency-applied current curve. We also show that equivalent results exist for constant and noisy point-source input to the dendrite. We note that the results are not specific to neurons but are applicable to any oscillator subject to a passive load.

DOI: [10.1103/PhysRevE.83.031906](https://doi.org/10.1103/PhysRevE.83.031906)

PACS number(s): 87.19.II, 87.19.In, 82.40.Bj

### I. INTRODUCTION

Neurons can have extensive spatial geometries, but they are often modeled as single-compartment objects that ignore the spatial anatomy of the cell. This simplification is made for mathematical tractability and computational efficiency. However, many neurons are not electrotonically compact, and single-compartment models cannot be expected to fully capture their behavior. Dendritic properties can have substantial effects on the dynamics of single neurons, as well as the activity in neuronal networks. For example, the architecture of a dendritic tree can alter the firing pattern and encoding properties of a neuronal oscillator [1–3] and dendritic filtering can change the phase-locking behavior in networks of neuronal oscillators [4–6]. Even the effects of dendrites without active ionic currents are not always straightforward. Intuitively, if the leakage reversal potential of the passive dendrite is lower than the average voltage of the oscillations, then the firing frequency of the neuronal oscillator will decrease with the addition of the dendrite [see Fig. 1(a)]. Surprisingly, however, the passive hyperpolarizing dendritic “load” can sometimes have very little effect on a neuron’s firing frequency [Fig. 1(c)] or even increase it [Fig. 1(b)] [7,8].

In previous modeling and experimental work, Kepler *et al.* [7] and Sharp *et al.* [8] examined the influence of electrical coupling between a neuronal oscillator and a passive cell, which is analogous to a two-compartment model of a soma with a passive dendrite [6]. They demonstrated that when the oscillator has a predominantly hyperpolarized membrane potential waveform (i.e., a short duty cycle), the electrical load of the passive cell acted to decrease the frequency of oscillations as the strength of the electrical coupling increased. On the other hand, when the oscillator had a predominantly depolarized membrane potential wave form (i.e., a long duty cycle), the electrical load of the passive cell acted to initially increase the frequency of oscillations as the strength

of electrical coupling increased until the frequency reached a maximum and then decreased with a further increase in coupling strength. In an analogous chemical oscillator system, Dolnik *et al.* [9] observed a similar frequency modulation when properties of the chemical load were altered rather than the wave form of the isolated oscillator.

Here, we extend the results of Kepler *et al.* by developing a general framework to understand the mechanisms by which dendritic load properties and intrinsic somatic properties affect the firing frequency of the neuronal oscillator. We model a neuron as an isopotential somatic oscillator attached to a thin passive dendritic cable using the “ball-and-stick” model [10], as well as an isopotential somatic oscillator compartment electrically coupled to a passive compartment, i.e., a two-compartment model (see Appendix D). We use the theory of weak coupling [11–13] to derive an equation for the change in the firing frequency of the neuron resulting from the presence of the dendritic load. We then show how the frequency effects of adding a dendrite to a neuronal oscillator can be understood in terms of dendritic properties and the somatic oscillator’s phase response curve (PRC). Finally, we link these effects to the shape of the oscillator’s frequency-applied current ( $f$ - $I$ ) curve.

### II. BALL-AND-STICK MODEL NEURON

We model the electrical activity of a neuron using a “ball-and-stick” model [4,5] that consists of a spherical active isopotential soma attached to a single thin passive dendrite. The dendrite is modeled as a one-dimensional passive cable of physical length  $L$  [14,15],

$$C_m \frac{\partial v}{\partial t} = \frac{a}{2R_C} \frac{\partial^2 v}{\partial x^2} - g_{LD}(v - E_{LD}), \quad x \in (0, L), \quad (1)$$

where  $v(x, t)$  is the voltage of the dendrite in mV at position  $x$  and time  $t$ ,  $g_{LD}$  is the leakage conductance in the dendrite in mS/cm<sup>2</sup>,  $R_C$  is the cytoplasmic resistivity of the dendrite in k $\Omega$  cm,  $a$  is the radius of the dendrite in cm,  $E_{LD}$  is the reversal potential of the leakage conductance in the dendrite

\*Corresponding author. Tel: +530-554-9394; fax: +530-752-6635.  
E-mail address: [tjlewis@ucdavis.edu](mailto:tjlewis@ucdavis.edu)

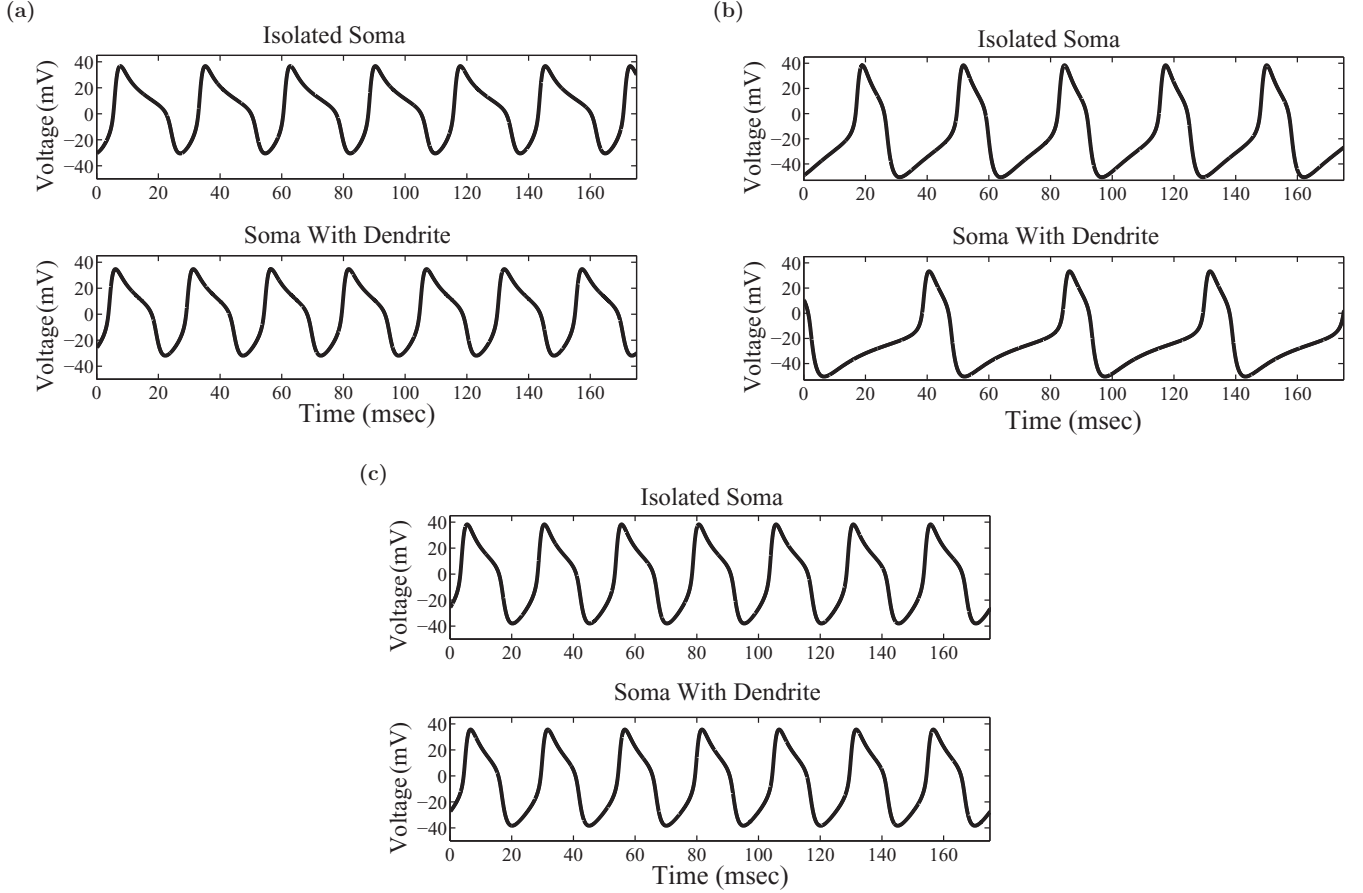


FIG. 1. The addition of a hyperpolarized dendrite can decrease, increase, or not change firing frequency. Voltage traces for a Morris-Lecar neuron without a dendritic cable [an isolated soma,  $\varepsilon(a) = 0$ ] and with a passive dendritic cable [ $\varepsilon(a) = 0.25$ ] for three different values of applied current to the soma: (a)  $I = 6.4 \mu\text{A}/\text{cm}^2$ , (b)  $I = 22.4 \mu\text{A}/\text{cm}^2$ , and (c)  $I = 16.6 \mu\text{A}/\text{cm}^2$ . In all cases, the dendritic leakage reversal potential  $E_{LD}$  is held at  $-60$  mV, which is hyperpolarized relative to the voltage oscillations. However, the frequency of the somatic oscillator decreases in (a), increases in (b), and changes by a negligible amount in (c).

in mV, and  $C_m$  is the membrane capacitance in  $\mu\text{F}/\text{cm}^2$ , which is assumed to be constant throughout the neuron.

Hodgkin-Huxley (HH) [16] type equations are used to model the electrical activity of the soma. An application of the conservation of current law at the junction connecting the spherical soma and the thin dendrite ( $x = 0$ ) yields the proximal boundary condition

$$C_m \frac{\partial v}{\partial t}(0, t) = -I_{\text{ion},s}[v(0), \vec{w}] + I + \frac{a^2}{d^2 R_C} \frac{\partial v}{\partial x}(0, t), \quad (2)$$

where  $I_{\text{ion},s}(v, \vec{w})$  represents the sum of the HH-type ionic currents (see Appendices A and B),  $\vec{w}$  is a vector containing the gating variables of the ionic conductances, and  $d$  is the diameter of the soma in cm. The gating variables in the vector  $\vec{w}$  are described by equations of the form  $\frac{d\vec{w}}{dt} = \frac{1}{\tau_{\vec{w}}} [\vec{w}_{\infty}(v) - \vec{w}]$ . The last term in Eq. (2) represents the axial current flowing from the dendrite into the soma. The parameter  $I$  is the somatic bias current in  $\mu\text{A}/\text{cm}^2$ . Note that changes in  $I$  are equivalent to changes in the leakage reversal potential,  $E_L$ , and therefore changes in  $I$  can be thought of as being caused by changes in current input at the soma or changes in the concentration of a neuromodulator. The values of  $I$  and  $E_L$  are chosen such

that the isolated soma undergoes  $T$ -periodic (limit cycle) oscillations. We define  $v_{LC}(t)$  to be the membrane potential component of the isolated somatic oscillator's limit cycle.

We assume that no current flows out the distal end of the dendrite, which yields the no-flux boundary condition at the end of the dendrite ( $x = L$ ),

$$\frac{\partial v}{\partial x}(L, t) = 0. \quad (3)$$

Note that this model is the ‘‘Rall lumped soma’’ model [10] with boundary conditions altered to include active conductances in the soma [5].

The Morris-Lecar model [17,18] and a neuron model of Traub [19,20] are used in the simulations presented here. However, similar results were obtained using several other model neurons [16,21–23]. Furthermore, the basic analysis that we present here is general and can be applied to any oscillator.

The analysis in this paper relies on a certain combination of model parameters being sufficiently ‘‘small.’’ To identify this small compound parameter, we nondimensionalize the model (1)–(3). We set  $V = V(\bar{x}, \bar{t}) = \frac{v(\lambda\bar{x}, \tau_S\bar{t}) - E_L}{-E_L}$  (where  $E_L$  is the leakage reversal potential in the soma),  $\bar{x} = \frac{x}{\lambda}$ ,  $\bar{t} = \frac{t}{\tau_S}$ , where  $\lambda(a) = \sqrt{\frac{a}{2R_C g_{LD}}}$  is the length constant of the dendrite,

and  $\tau_S = \frac{C_m}{g_L}$  is the membrane time constant of the soma. The resulting nondimensional equations for the ball-and-stick model neuron are

$$g \frac{\partial V}{\partial \bar{t}} = \frac{\partial^2 V}{\partial \bar{x}^2} - (V - \bar{E}_{LD}), \quad (4)$$

$$\frac{\partial V}{\partial \bar{t}}(0, \bar{t}) = -\bar{I}_{\text{ion},S}[V(0, \bar{t}), \bar{w}] + \bar{I} + \varepsilon(a) \frac{\partial V}{\partial \bar{x}}(0, \bar{t}), \quad (5)$$

$$\frac{\partial V}{\partial \bar{x}} \left( \frac{L}{\lambda(a)}, \bar{t} \right) = 0, \quad (6)$$

where  $g = \frac{g_L}{g_{LD}}$ ,  $\bar{E}_{LD} = \frac{E_{LD} - E_L}{-E_L}$ ,  $\bar{I}_{\text{ion},S}[V(0, \bar{t}), \bar{w}] = \frac{1}{-g_L E_L} I_{\text{ion},S}[-E_L V(0, \bar{t}) + E_L, \bar{w}]$ ,  $\bar{I} = \frac{1}{-g_L E_L} I$ , and  $\varepsilon(a) = \frac{a^2}{d^2 g_L R_C \lambda(a)}$ . Also,  $\frac{d\bar{w}}{d\bar{t}} = \frac{1}{\tau_w} [\bar{w}_\infty(v) - \bar{w}]$  becomes  $\frac{d\bar{w}}{d\bar{t}} = \frac{\tau_S}{\tau_w} [\bar{w}_\infty(-E_L V(0, \bar{t}) + E_L) - \bar{w}]$ . We define the nondimensionalized period of the limit cycle to be  $\bar{T} = \frac{T}{\tau_S}$ , and the nondimensional voltage component of the isolated soma's limit cycle as  $V_{LC}(\bar{t})$ .

The term  $\varepsilon(a) \frac{\partial V}{\partial \bar{x}}(0, \bar{t})$  in Eq. (5) is the nondimensional axial current at the soma-dendritic junction and is the dendrite's perturbation to the somatic membrane dynamics. To ensure that this perturbation is weak, we assume that

$$\varepsilon(a) = \frac{a^2}{d^2} \sqrt{\frac{2g_{LD}}{g_L^2 R_C a}} = \left( \pi a^{3/2} \sqrt{\frac{2g_{LD}}{R_C}} \right) \left( \frac{1}{g_L \pi d^2} \right)$$

is small. Essentially, we assume that  $a \ll d$ , i.e., that the radius of the dendrite is small relative to the diameter of the soma, and that  $\sqrt{\frac{2g_{LD}}{g_L^2 R_C a}}$  is  $O(1)$  so that  $\varepsilon(a) \ll 1$ . Note that  $\varepsilon(a)$  is the input conductance of the dendrite at the soma if it was of infinite length normalized by the total membrane conductance of the soma.

### III. THEORY OF WEAK COUPLING AND REDUCTION TO A PHASE MODEL

The theory of weak coupling [11–13] has been widely used to analyze dynamics in networks of oscillating neurons (e.g., Refs. [24–27]). The theory can also be used to analyze the dynamics of neurons under the influence of an external forcing. When this perturbing current to an individual neuron is sufficiently weak, the complete state of the neuron can be approximated by its phase on its  $\bar{T}$ -periodic limit cycle,  $\theta(\bar{t}) \in [0, 1)$ . Furthermore, the evolution of the neuronal oscillator's phase is governed by its phase equation,

$$\frac{d\theta}{d\bar{t}} = \bar{\omega} + \Delta\bar{\omega} = \bar{\omega} + \frac{1}{\bar{T}} \int_0^{\bar{T}} Z(s) I_{\text{pert}}(s) ds, \quad (7)$$

where  $\frac{d\theta}{d\bar{t}}$  is the instantaneous nondimensional frequency of the neuron, and  $\bar{\omega} = \frac{1}{\bar{T}}$  is the nondimensional frequency of the isolated (unperturbed) somatic oscillator.  $I_{\text{pert}}(s)$  is a nondimensional  $\bar{T}$ -periodic perturbing current that can be thought of as arising from coupling (e.g., coupling to a dendritic load) and/or external input.  $Z(s)$  is the nondimensional infinitesimal PRC of the neuronal oscillator. The PRC quantifies the change in phase resulting from a  $\delta$ -function current perturbation at a particular phase on the limit cycle. The PRC can be

thought of as a Green's function or impulse response function for a linear oscillator.  $\Delta\bar{\omega} = \frac{1}{\bar{T}} \int_0^{\bar{T}} Z(s) I_{\text{pert}}(s) ds$  represents the modulation of the isolated oscillator's frequency caused by the external current averaged over one period of the oscillations.

The theory of weak coupling can be applied to the ball-and-stick model by considering the dendritic load as the perturbation to the soma, following Crook *et al.* [5]. During steady oscillations in the ball-and-stick model, a  $\bar{T}$ -periodic current flows between the soma and dendrite, modulating the intrinsic oscillations of the soma. Therefore, we set  $I_{\text{pert}}(s) = \varepsilon(a) \frac{\partial V}{\partial \bar{x}}(0, s)$ , which is the (nondimensional) current at the soma-dendritic junction. As long as this modulating current is sufficiently weak, the dynamics of the ball-and-stick model can be reduced to the phase model

$$\frac{d\theta}{d\bar{t}} = \bar{\omega} + \frac{1}{\bar{T}} \int_0^{\bar{T}} Z(s) \varepsilon(a) \frac{\partial V}{\partial \bar{x}}(0, s) ds. \quad (8)$$

In order to close Eq. (8),  $\frac{\partial V}{\partial \bar{x}}(0, \bar{t})$  needs to be determined. Using our assumption that  $\varepsilon(a) \ll 1$ , we can find a leading-order approximation of  $\frac{\partial V}{\partial \bar{x}}(0, \bar{t})$ . Because the dendritic perturbation is weak, the soma clings tightly to its limit cycle so that  $V(0, \bar{t}) \simeq V_{LC}(\bar{t})$ . This approximation simplifies the boundary condition at the soma ( $\bar{x} = 0$ ) and yields the leading-order approximation for the system (4)–(6):

$$g \frac{\partial V}{\partial \bar{t}} = \frac{\partial^2 V}{\partial \bar{x}^2} - (V - \bar{E}_{LD}), \quad (9)$$

$$V(0, \bar{t}) = V_{LC}(\bar{t}), \quad (10)$$

$$\frac{\partial V}{\partial \bar{x}} \left[ \frac{L}{\lambda(a)}, \bar{t} \right] = 0. \quad (11)$$

System (9)–(11) is a first-order linear partial differential equation with  $\bar{T}$ -periodic forcing at one end, and the solution can be found using a Fourier series. Expanding the somatic potential in a Fourier series,  $V_{LC}(\bar{t}) = \frac{1}{\bar{T}} \sum_{n \in \mathbb{Z}} V_n e^{2\pi i n \bar{t} / \bar{T}}$ , and solving system (9)–(11) yields

$$V(\bar{x}, \bar{t}) = \left( \frac{V_0}{\bar{T}} - \bar{E}_{LD} \right) \frac{\cosh \left[ \bar{x} - \frac{L}{\lambda(a)} \right]}{\cosh \left[ \frac{L}{\lambda(a)} \right]} + \frac{1}{\bar{T}} \sum_{n \neq 0} V_n \frac{\cosh \left\{ b_n \left[ \bar{x} - \frac{L}{\lambda(a)} \right] \right\}}{\cosh \left\{ b_n \left[ \frac{L}{\lambda(a)} \right] \right\}} e^{2\pi i n \bar{t} / \bar{T}} + \bar{E}_{LD}, \quad (12)$$

where  $b_n = \sqrt{1 + g 2\pi i n / \bar{T}}$ . Differentiating Eq. (12) with respect to  $\bar{x}$  and evaluating at  $\bar{x} = 0$  gives

$$\frac{\partial V}{\partial \bar{x}}(0, \bar{t}) = \left( \bar{E}_{LD} - \frac{V_0}{\bar{T}} \right) c_0(a) - \frac{1}{\bar{T}} \sum_{n \neq 0} c_n(a) V_n e^{2\pi i n \bar{t} / \bar{T}}, \quad (13)$$

where  $c_n(a) = b_n \tanh[b_n \frac{L}{\lambda(a)}]$ . Note that  $c_n(a)$  are complex numbers that capture the “filtering” effects of the dendrite.

Substituting this expression for  $\frac{\partial V}{\partial \bar{x}}(0, \bar{t})$  back into Eq. (8) and expanding the PRC in a Fourier series,  $Z(\bar{t}) = \frac{1}{\bar{T}} \sum_{m \in \mathbb{Z}} Z_m e^{2\pi i m \bar{t} / \bar{T}}$ , yields the phase model for the

ball-and-stick model,

$$\begin{aligned} \frac{d\theta}{d\bar{t}} &= \bar{\omega} + \Delta\bar{\omega} = \bar{\omega} + \varepsilon(a) \left[ \frac{Z_0}{\bar{T}} \left( \bar{E}_{LD} - \frac{V_0}{\bar{T}} \right) c_0(a) - \frac{1}{\bar{T}^2} \sum_{n \neq 0} Z_{-n} V_n c_n(a) \right] \\ &= \bar{\omega} + \varepsilon(a) \left[ \frac{Z_0}{\bar{T}} \left( \bar{E}_{LD} - \frac{V_0}{\bar{T}} \right) c_0(a) - \frac{2}{\bar{T}^2} \sum_{n=1}^{\infty} |Z_n V_n c_n(a)| \cos(\psi_n(a) + \gamma_n - \phi_n) \right], \end{aligned} \quad (14)$$

where  $\psi_n(a)$ ,  $\gamma_n$ , and  $\phi_{-n}$  are the angles, in radians, corresponding to  $c_n(a)$ ,  $V_n$ , and  $Z_{-n}$ , respectively.

Below we will analyze the phase model in order to understand how the addition of the thin passive dendrite alters

the frequency of the somatic oscillator. For convenience of physiological interpretation, the values of all quantities are reported in dimensional terms in the results section. The phase model in dimensional terms is

$$\frac{d\theta}{dt} = \omega + \Delta\omega = \omega + \frac{\varepsilon(a)}{\tau_S} \left[ \langle z \rangle (E_{LD} - \langle v_{LC} \rangle) c_0(a) - \frac{2}{T^2} \sum_{n=1}^{\infty} |z_n v_n c_n(a)| \cos(\psi_n(a) + \gamma_n - \phi_n) \right], \quad (15)$$

where  $v_n$  and  $z_n$  are the Fourier coefficients of the membrane potential oscillations  $v_{LC}(t)$  and the dimensional PRC  $z(t)$ , respectively, and  $\langle v_{LC} \rangle = v_0/T$  and  $\langle z \rangle = z_0/T$  are the mean values of  $v_{LC}(t)$  and  $z(t)$ , respectively.

In Appendix E, we show how input from point sources on the dendrite can be incorporated into Eq. (15) and demonstrate that including point sources with constant input is equivalent to changing  $E_{LD}$ . Furthermore, this result can be extended to noisy input on the dendrites when the noise is exponentially correlated with a sufficiently large time constant [28].

#### IV. RESULTS

In this section, we examine the dependence of firing frequency of the ball-and-stick neuron on the magnitude of the dendritic perturbation  $\varepsilon(a)$  and the value of  $E_{LD}$ . We emphasize the fact that changes in the bias current,  $I$ , can be thought of as either changes in the leakage reversal potential of the soma,  $E_L$  or current input to the soma; also changes in the leakage reversal potential of the dendrite,  $E_{LD}$ , can be thought of as arising from either global changes in dendritic leakage reversal potential, or point-source synaptic inputs to the dendrite (Appendix E). First, we observe the behavior of the simulated model equations (1)–(3), and we show that this behavior is well approximated by the phase model (15). We then interpret this behavior in terms of the biophysical quantities in Eq. (15):  $\langle z \rangle$ ,  $\langle v_{LC} \rangle$ ,  $E_{LD}$ ,  $\varepsilon(a)$ ,  $c_n(a)$ ,  $v_n$ , and  $z_n$ . Lastly, we illustrate a connection between two intrinsic properties of the isolated neuronal oscillator: the frequency-applied current curve and the average value of the PRC.

In all simulations, unless otherwise indicated, somatic dynamics are modeled by the Morris-Lecar equations with parameters given in the Appendix A. We also view an increase in  $\varepsilon(a)$  as an increase in the dendritic radius  $a$ . Note, however, that an increase in  $a$  also results in an increase the dendritic space constant,  $\lambda(a)$ .

##### A. Simulations: Passive dendritic load can either increase or decrease firing frequency

Figure 1 plots the somatic voltage traces for two different values of applied current to the soma,  $I = 6.4 \mu\text{A}/\text{cm}^2$  [Fig. 1(a)] and  $I = 22.4 \mu\text{A}/\text{cm}^2$  [Fig. 1(b)]. For both cases,  $E_{LD}$  is set to  $-60$  mV, which is hyperpolarized relative to the somatic membrane potential. Intuitively, we expect that the hyperpolarizing dendritic load should decrease the frequency of the oscillations. This is clearly the case in Fig. 1(a) in which the frequency of the isolated somatic oscillator is greater than the frequency of the oscillator attached to the dendrite. However, in Fig. 1(b), the frequency of the isolated somatic oscillator is lower than the frequency when the somatic oscillator is attached to the dendrite. Furthermore, the frequency of the oscillator can remain unchanged [Fig. 1(c)] with the addition of the dendrite. Thus, simply by varying the current applied to the soma, the hyperpolarizing dendritic load can have a decelerating, accelerating, or negligible effect on the frequency of oscillations. As mentioned earlier, this phenomenon is similar to what Kepler *et al.* [7] observed in a model of a neuronal oscillator electrically coupled to a passive cell.

Figure 2 shows the change in firing frequency of the full ball-and-stick model (dotted line) as a function of  $\varepsilon(a)$  with  $I = 6.4 \mu\text{A}/\text{cm}^2$  and  $I = 22.4 \mu\text{A}/\text{cm}^2$  for two different values of  $E_{LD}$ . For a relatively hyperpolarized value of  $E_{LD}$  ( $-75$  mV), the frequency of oscillations decreases as  $\varepsilon(a)$  is increased for  $I = 6.4 \mu\text{A}/\text{cm}^2$  [Fig. 2(a)], but the frequency increases as  $\varepsilon(a)$  is increased for  $I = 22.4 \mu\text{A}/\text{cm}^2$  [Fig. 2(a)]. This agrees with the behavior seen in Fig. 1. When the value of  $E_{LD}$  is relatively depolarized (i.e.,  $E_{LD} = 25$  mV, which is close to the peak of the somatic voltage), the results are reversed. That is, the frequency of oscillations increases as  $\varepsilon(a)$  is increased for  $I = 6.4 \mu\text{A}/\text{cm}^2$  and decreases as  $\varepsilon(a)$  is increased for  $I = 22.4 \mu\text{A}/\text{cm}^2$ . Thus, the results in Fig. 2(a) agree with our intuition about the

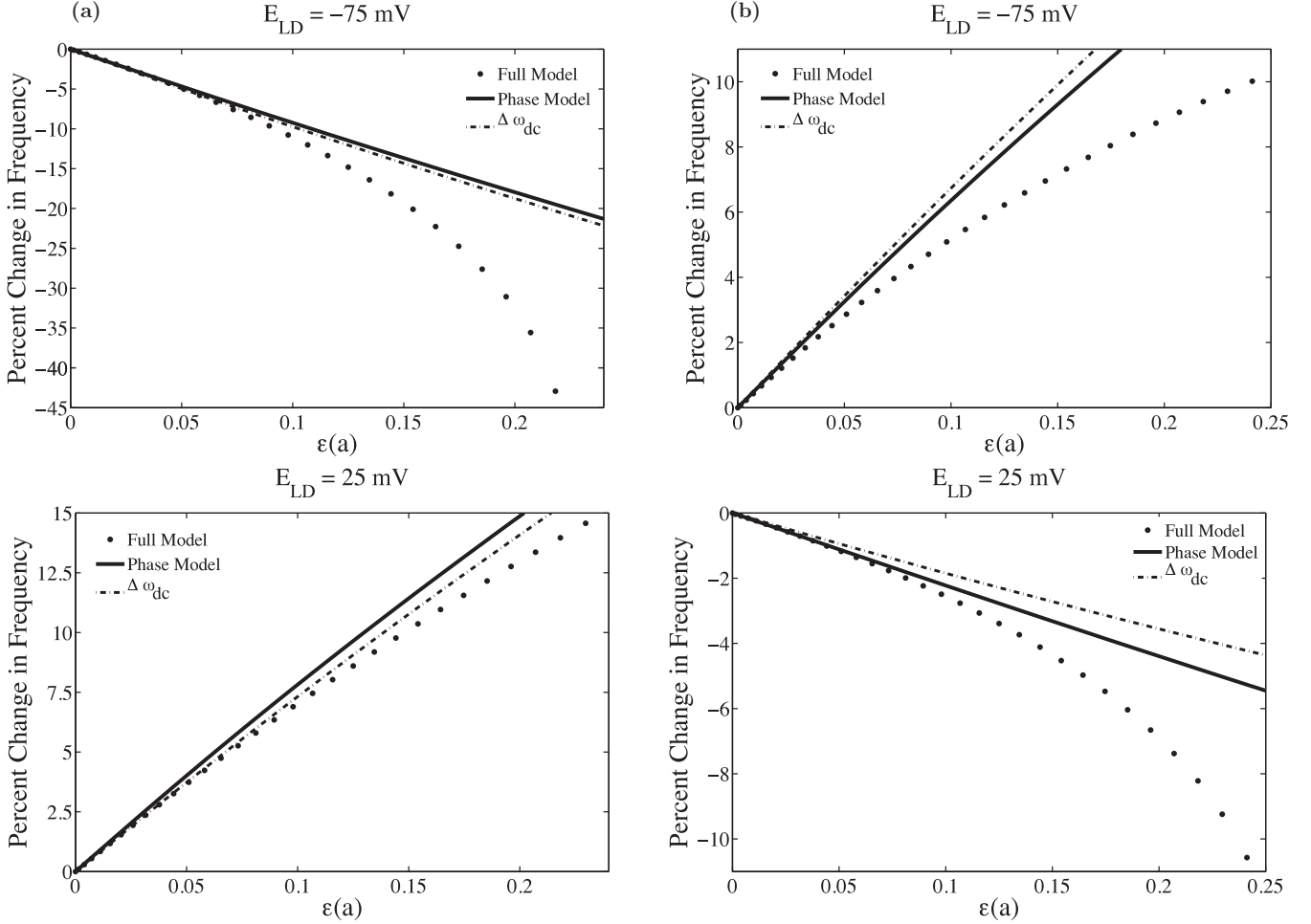


FIG. 2. Firing frequency can either increase or decrease as a function of increasing magnitude of the dendritic perturbation,  $\varepsilon(a)$ , depending upon the value of the dendritic leakage reversal potential and the applied current at the soma. The percent change in firing frequency is plotted as a function of the strength of the dendritic perturbation,  $\varepsilon(a)$ , for hyperpolarized ( $-75$  mV) and depolarized ( $25$  mV) values of  $E_{LD}$  when (a)  $I = 6.4 \mu\text{A}/\text{cm}^2$  and (b)  $I = 22.4 \mu\text{A}/\text{cm}^2$ . The dots represent results from simulations of the full ball-and-stick model, Eqs. (1)–(3), the solid line represents results from simulations of the phase model, Eq. (15), and the dashed-dotted line represents  $\Delta\omega_{dc}$ , Eq. (16). In (a), the addition of the dendrite with a hyperpolarized (depolarized) leakage reversal potential decrease (increases) the frequency of oscillations as  $\varepsilon(a)$  is increased. In (b), we see the opposite effect: the addition of the dendrite with a hyperpolarized (depolarized) leakage reversal potential increases (decreases) the frequency of oscillations as  $\varepsilon(a)$  is increased. Note that, for all four plots,  $\Delta\omega_{dc}$  captures the tendency for the frequency to increase or decrease as a function of  $\varepsilon(a)$ .

effects of dendritic load: When the leakage reversal potential of the dendrite is hyperpolarized (depolarized) relative to the somatic voltage oscillations, the frequency of oscillations is decreased (increased) as the strength of the dendritic perturbation is increased. However, Fig. 2(b) shows that by changing the intrinsic period of the somatic oscillator, the addition of a passive hyperpolarizing dendrite load can have a counterintuitive effect and increase the frequency of oscillations.

### B. Mechanisms for frequency changes: Insights from the phase model

The phase model quantitatively captures the behavior of the full model for sufficiently small values of  $\varepsilon(a)$ , and Fig. 2 shows that it can also capture the qualitative behavior for

moderate values of  $\varepsilon(a)$ . Therefore, we can use the phase model to explain the effects of dendritic load on firing frequency in terms of cable properties and intrinsic properties of the neuronal oscillator. To do this, it is useful to emphasize the split in the frequency modulation term of the phase model  $\Delta\omega$  into the dc ( $n = 0$ ) component  $\Delta\omega_{dc}$  and the ac ( $n \neq 0$ ) component  $\Delta\omega_{ac}$ . That is,  $\Delta\omega = \Delta\omega_{dc} + \Delta\omega_{ac}$ , where

$$\Delta\omega_{dc} = \frac{\varepsilon(a)}{\tau_S} \langle z \rangle (E_{LD} - \langle v_{LC} \rangle) c_0(a), \quad (16)$$

$$\Delta\omega_{ac} = -\frac{\varepsilon(a)}{\tau_S} \frac{2}{T^2} \sum_{n=1}^{\infty} |z_n v_n c_n(a)| \cos(\psi_n(a) + \gamma_n - \phi_n). \quad (17)$$

Note that the dc components  $\Delta\omega_{dc}$  corresponding to the examples depicted in Fig. 2 accurately capture the tendency

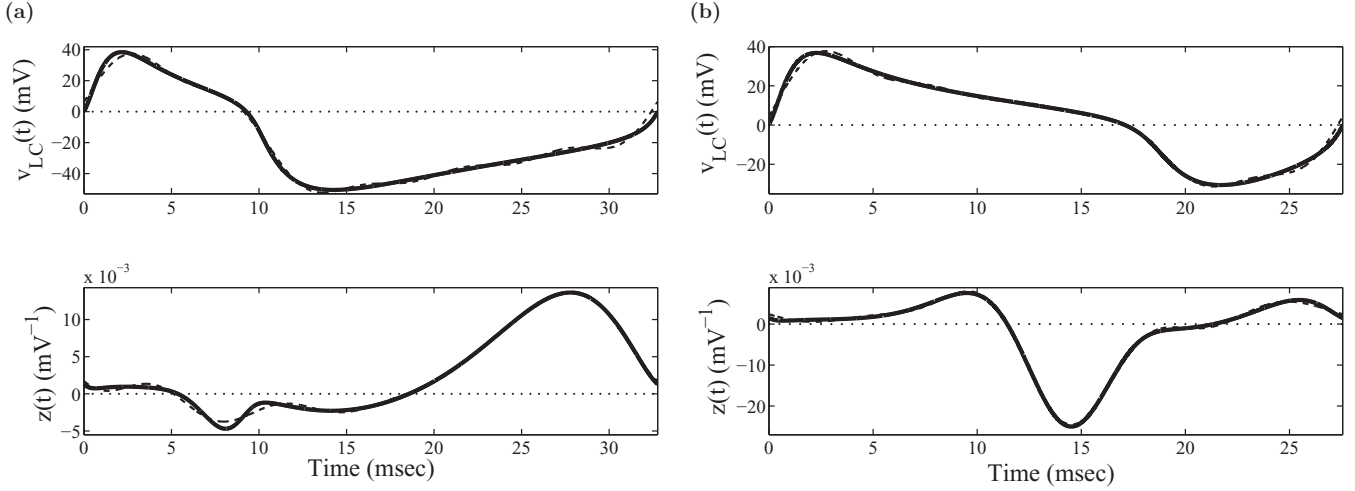


FIG. 3. Voltage component of the limit cycle for the Morris-Lecar neuron and its corresponding phase response curve. (a)  $I = 6.4 \mu\text{A}/\text{cm}^2$  and (b)  $I = 22.4 \mu\text{A}/\text{cm}^2$ . The oscillator in (a) has a positive average value of its phase response curve  $\langle z \rangle = 0.0027 \text{ mV}^{-1}$  and a mean membrane potential of  $\langle v_{LC} \rangle = -17.9 \text{ mV}$ , while the oscillator in (b) has  $\langle z \rangle = -0.0016 \text{ mV}^{-1}$  and  $\langle v_{LC} \rangle = 3.5 \text{ mV}$ . The dashed line in all plots is the approximation to the function using the first five Fourier modes in its expansion.

for the frequency to increase or decrease as a function of  $\varepsilon(a)$ . Given that the dc component plays the dominant role in determining the frequency modulation, Eq. (16) reveals the mechanisms underlying the phenomena described in the previous sections. Specifically, the tendency for the frequency of the oscillations to increase or decrease as a function of  $\varepsilon(a)$  is determined by the sign of the product of  $\langle z \rangle$  and  $(E_{LD} - \langle v_{LC} \rangle)$ . [Note that  $c_0(a) = \tanh[L/\lambda(a)]$  is real and positive]. In Fig. 3, it can be seen that (a) for  $I = 6.4 \mu\text{A}/\text{cm}^2$ , the average value of the PRC is positive ( $\langle z \rangle = 0.0027 \text{ mV}^{-1}$ ), whereas (b) for  $I = 22.4 \mu\text{A}/\text{cm}^2$ , the average value of the PRC is negative ( $\langle z \rangle = -0.0016 \text{ mV}^{-1}$ ). Therefore, when  $E_{LD}$  is less than  $\langle v_{LC} \rangle$  (i.e., the dendritic load is hyperpolarizing), the frequency of oscillations decreases in case (a) but increases in case (b) as  $\varepsilon(a)$  increases. When  $E_{LD}$  is greater than  $\langle v_{LC} \rangle$ , the results are reversed. This simple explanation accounts for all of the behavior in Fig. 2, and it will hold in general whenever  $\Delta\omega_{dc}$  is the dominant term in  $\Delta\omega$ , i.e., whenever  $\langle z \rangle$  is not close to zero and/or  $\langle v_{LC} \rangle$  is not close to  $E_{LD}$ .

$\Delta\omega_{dc}$  [Eq. (16)] predicts that the effect of the dendritic load will switch between decelerating and accelerating as  $E_{LD}$  crosses  $\langle v_{LC} \rangle$ . Figure 4 plots the change in firing frequency as a function of  $E_{LD}$  for the full model (dotted line), the phase model (solid line), and the  $\Delta\omega_{dc}$  prediction (dashed line) for three different applied currents: (a)  $I = 6.4 \mu\text{A}/\text{cm}^2$  where  $\langle z \rangle > 0$ , (b)  $I = 22.4 \mu\text{A}/\text{cm}^2$  where  $\langle z \rangle < 0$ , and (c)  $I = 16.6 \mu\text{A}/\text{cm}^2$  where  $\langle z \rangle$  is negative but is two orders of magnitude smaller than that in (b). As expected from the signs of  $\langle z \rangle$ , the dendritic load changes from having a decelerating effect to an accelerating effect in case (a) and an accelerating effect to a decelerating effect in case (b) as  $E_{LD}$  is increased.  $\Delta\omega_{dc}$  predicts that the switch occurs at  $\langle v_{LC} \rangle = -17.9 \text{ mV}$  for (a) and  $\langle v_{LC} \rangle = 3.5 \text{ mV}$  for (b). These are close to the actual switching points, which are  $E_{LD} \sim -22 \text{ mV}$  in (a) and  $E_{LD} \sim 0 \text{ mV}$  in (b). Note that  $\langle z \rangle$  does not only predict the increase and/or decrease in frequency, but it is also a measure of the sensitivity of the neuronal oscillator to the dendritic load.

In the cases portrayed in Figs. 4(a) and 4(b),  $\Delta\omega_{dc}$  does an excellent job of predicting both the sign and magnitude of the change in frequency over a broad range of  $E_{LD}$ . However, as  $E_{LD}$  approaches  $\langle v_{LC} \rangle$ , the magnitude of the dc component becomes smaller than the ac component. As a consequence,  $\Delta\omega_{dc}$  incorrectly predicts the sign of frequency change in the interval between the actual and the predicted switching points. The size of this “interval of error” for the dc prediction is

$$|E_{LD} - \langle v_{LC} \rangle| = \frac{\tau_S}{\varepsilon(a)} \frac{|\Delta\omega_{ac}|}{\langle z \rangle c_0(a)} = \frac{2}{T^2} \frac{\sum_{n=1}^{\infty} |z_n v_n c_n(a)| \cos(\psi_n(a) + \gamma_n - \phi_n)}{\langle z \rangle c_0(a)}. \quad (18)$$

The relative magnitude of  $\langle z \rangle$  as compared to the ac component in the cases in Figs. 4(a) and 4(b) is small and makes the interval of error small (3.5 and 3.8 mV, respectively). However, for different parameters,  $\langle z \rangle$  can be relatively small and  $\Delta\omega_{ac}$  can be the dominant term in  $\Delta\omega$ . This can cause the interval of error to be large. For example, in Fig. 4(c), where  $\langle z \rangle = -4.31 \times 10^{-5} \text{ mV}^{-1}$ , the size of the interval of error is 132.6 mV.

Over the range of applied currents tested ( $4.4$ – $23.6 \mu\text{A}/\text{cm}^2$ ),  $\langle z \rangle$  monotonically decreases from  $0.0074$  to  $-0.0036 \text{ mV}^{-1}$ , and the magnitude of the normalized ac components  $|\frac{\Delta\omega_{ac}}{\varepsilon(a)}|$  ranges from  $0.0059$  to  $0.027$  for  $a = 2 \times 10^{-6} \text{ cm}$  [ $\varepsilon(a) = 0.01118$ ]. Furthermore,  $c_0(a) \sim 1$  and the magnitude of the normalized ac components  $\frac{\Delta\omega_{ac}}{\varepsilon(a)}$  has a weak dependence on  $a$  for the parameters that we considered [i.e.,  $T \gg \tau_S$  and  $L > 1.5\lambda(a)$ ; see Appendix C]. As a result, the size of the interval of error for the dc prediction ranges from less than 1 mV near the edges of the applied current range to infinite when  $\langle z \rangle = 0$  near  $I = 16 \mu\text{A}/\text{cm}^2$ . The range of the applied current over which the size of the interval of error was greater than 20 mV is  $14.4$ – $17.6 \mu\text{A}/\text{cm}^2$ . Within this range, the frequency modulation primarily results from the

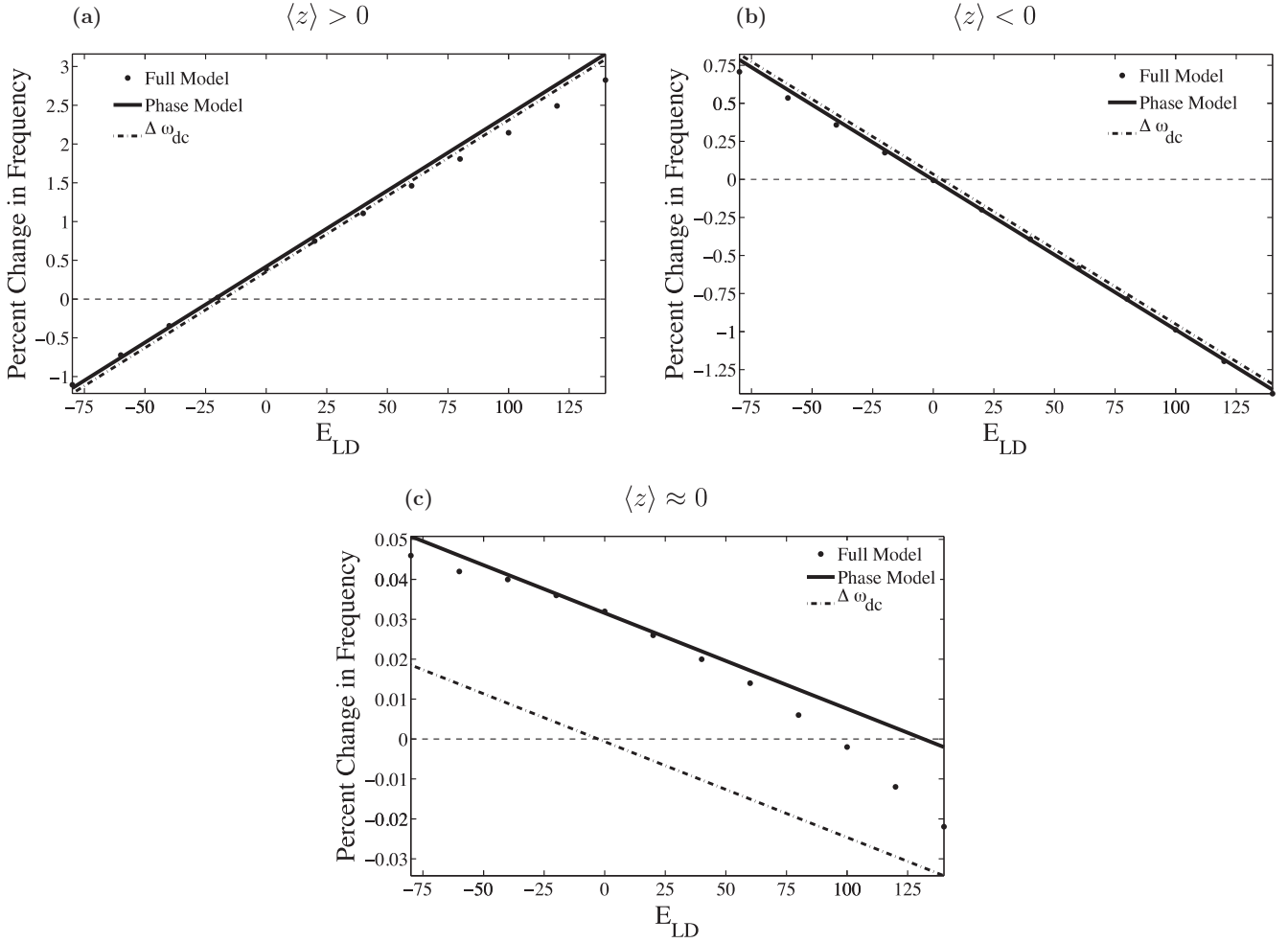


FIG. 4. Dendritic load switches its effect on frequency as the dendritic leakage reversal potential is increased. The percent change in firing frequency is plotted as a function of the dendritic leakage reversal potential,  $E_{LD}$ , for fixed  $\varepsilon(a) = 0.01118$  when (a)  $\langle z \rangle > 0$  ( $I = 6.4 \mu\text{A}/\text{cm}^2$ ), (b)  $\langle z \rangle < 0$  ( $I = 22.4 \mu\text{A}/\text{cm}^2$ ), and (c)  $\langle z \rangle \approx 0$  ( $I = 16.6 \mu\text{A}/\text{cm}^2$  and  $\langle z \rangle = -4.31 \times 10^{-5} \text{ mV}^{-1}$ ). The dots represent simulations of full ball-and-stick model [Eqs. (1)–(3)], the solid line represents simulations of the phase equation (15), and the dashed-dotted line represents  $\Delta\omega_{dc}$  [Eq. (16)]. In (a), the dendritic load switches from having a decelerating effect on frequency to an accelerating effect as  $E_{LD}$  is increased, while in (b), the dendritic load switches from having an accelerating effect on frequency to a decelerating effect as  $E_{LD}$  is increased. In both cases, the “interval of error” in which  $\Delta\omega_{dc}$  incorrectly predicts the sign of frequency change is small, and  $\Delta\omega_{dc}$  remains close to the full phase model prediction. When  $\langle z \rangle \approx 0$  as in (c), the interval of error is considerably larger. However, the frequency modulation effects are much smaller in (c) than in either (a) or (b).

ac component and is very weak, i.e.,  $\Delta\omega$  is on the order of  $0.01\varepsilon(a)$ . The dependence of frequency modulation on  $E_{LD}$  in this range is also very weak, as is seen in Figs. 4(c) and 5 and by the fact that  $\Delta\omega_{ac}$  is independent of  $E_{LD}$ .

### C. Average value of PRC and frequency-applied current ( $f$ - $I$ ) curve

The above results describe the mechanisms of frequency modulation caused by the dendrite in terms of the average value of the phase response curve  $\langle z \rangle$ , which is not a commonly considered quantity. Here, we derive the relationship between the familiar frequency-applied current ( $f$ - $I$ ) curve and the average value of the oscillator’s phase response curve, and we then link to this relationship back to the frequency effects of the passive dendrite on neuronal oscillations.

Consider an isolated neuronal oscillator subjected to a constant applied current  $I$ , and suppose that  $\omega(I)$  and  $z(s; I)$

are parametrizations of the frequency and PRC of the oscillator in terms of the applied current. Now suppose that applied current is increased by a small amount  $\Delta I$ . According to the theory of weak coupling, the new frequency of the oscillator is

$$\omega(I + \Delta I) = \frac{d\theta}{dt} \simeq \omega(I) + \frac{1}{T} \int_0^T z(s; I) \frac{\Delta I}{C_m} ds \quad (19)$$

$$= \omega(I) + \langle z(\cdot; I) \rangle \frac{\Delta I}{C_m}. \quad (20)$$

Rearranging Eq. (20) yields the relationship between the change in the frequency of an oscillator resulting from the additional applied current and average value of the oscillator’s PRC:

$$\frac{d\omega}{dI} \simeq \frac{1}{C_m} \frac{\omega(I + \Delta I) - \omega(I)}{\Delta I} = \frac{1}{C_m} \langle z(\cdot; I) \rangle. \quad (21)$$

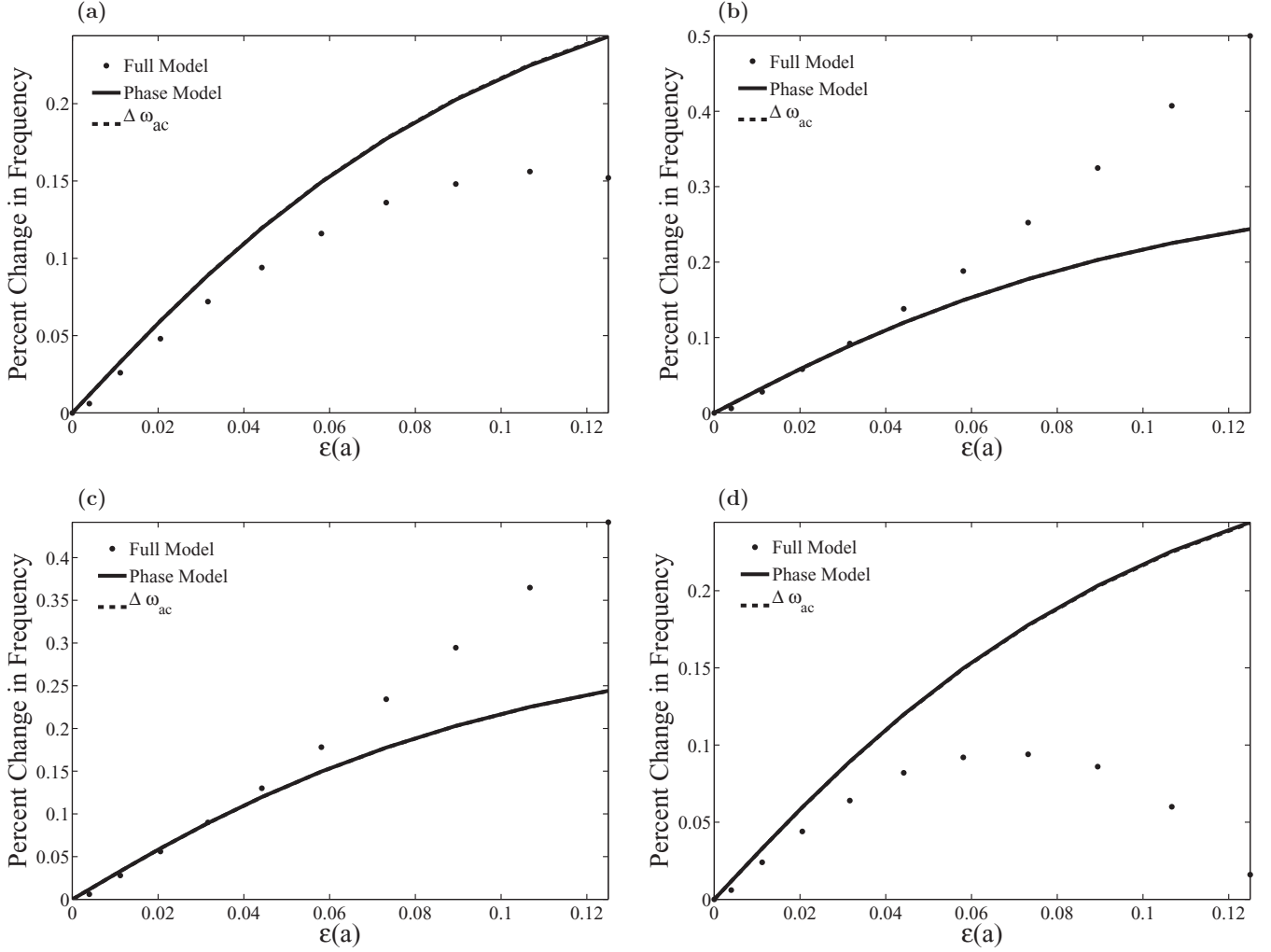


FIG. 5. When the average value of the PRC  $\langle z \rangle \approx 0$ ,  $\Delta\omega_{ac}$  dominates the behavior of the phase model. The percent change in firing frequency is plotted as a function of  $\varepsilon(a)$  when  $\langle z \rangle \approx 0$  ( $I = 16.32 \mu\text{A}/\text{cm}^2$  and  $\langle z \rangle = 1.39 \times 10^{-7} \text{ mV}^{-1}$ ) and  $E_{LD}$  is (a)  $-60 \text{ mV}$ , (b)  $-10 \text{ mV}$ , (c)  $15 \text{ mV}$ , and (d)  $55 \text{ mV}$ . The dots represent simulations of full ball-and-stick model [Eqs. (1)–(3)]. The simulations of the phase equation (15) (solid line) and  $\Delta\omega_{ac}$  [Eq. (16)] (the dashed line) overlap for the four values of the dendritic leakage reversal potential  $E_{LD}$ , indicating that  $\Delta\omega \simeq \Delta\omega_{ac}$  in this case. This is owing to the fact that  $\Delta\omega_{dc}$  is close to zero as  $\langle z \rangle \approx 0$ . Also, because  $\Delta\omega_{ac}$  is independent of  $E_{LD}$ , the phase model behavior remains virtually unchanged for the four different values of  $E_{LD}$ . Note that the frequency modulation effects of the dendrite are smaller than those seen in Fig. 2.

Thus, the average value of an oscillator's phase response curve for a particular value of applied current normalized by the membrane capacitance is equivalent to the instantaneous slope of the oscillator's  $f$ - $I$  curve at that particular applied current value. That is,  $\langle z \rangle$  is a measure of the sensitivity of the neuron to constant input and is proportional to the gain of the neuron. [Note that the right-hand side of Eq. (20) is a Taylor series of  $\omega(I + \Delta I)$  with  $\frac{d\omega}{dI} = \frac{\langle z(\cdot; I) \rangle}{C_m}$ ].

In the typical case where the dc component  $\Delta\omega_{dc}$  dominates the effect of the dendrite on firing frequency, we can substitute  $C_m \frac{d\omega}{dI}$  for  $\langle z(\cdot; I) \rangle$  into Eq. (16) to obtain

$$\begin{aligned}
 \frac{d\theta}{dt} &\simeq \omega + \frac{\varepsilon(a)}{\tau_S} C_m \frac{d\omega}{dI} (E_{LD} - \langle v_{LC} \rangle) c_0(a) \\
 &\simeq \omega + \frac{d\omega}{dI} [\varepsilon(a) c_0(a) g_L] (E_{LD} - \langle v_{LC} \rangle). \quad (22)
 \end{aligned}$$

Recall that  $I$  is the current applied to the soma per unit surface area of the soma. The term  $\varepsilon(a) c_0(a) g_L$  is the input conductance of the dendrite at the soma normalized to the surface area of the soma, and  $E_{LD} - \langle v_{LC} \rangle$  is the average difference between the membrane potentials of the soma and dendrite. That is, the change in frequency of a neuronal oscillator resulting from the addition of a passive dendrite is simply given by the product of the average axial current flowing between the dendrite and the soma (i.e., a *constant* current) and the slope of the neuronal oscillator's  $f$ - $I$  curve.

Figure 6(a) illustrates the relationship between the  $f$ - $I$  curve, its derivative, and the average of the PRC  $\langle z \rangle$  for the isolated Morris-Lecar neuron (i.e., the soma) as a function of applied current. For this model neuron, the  $f$ - $I$  curve is nonmonotonic: The frequency initially increases with increasing current, but the frequency reaches a maximum and then decreases with increasing current. As a result, the addition of a strictly

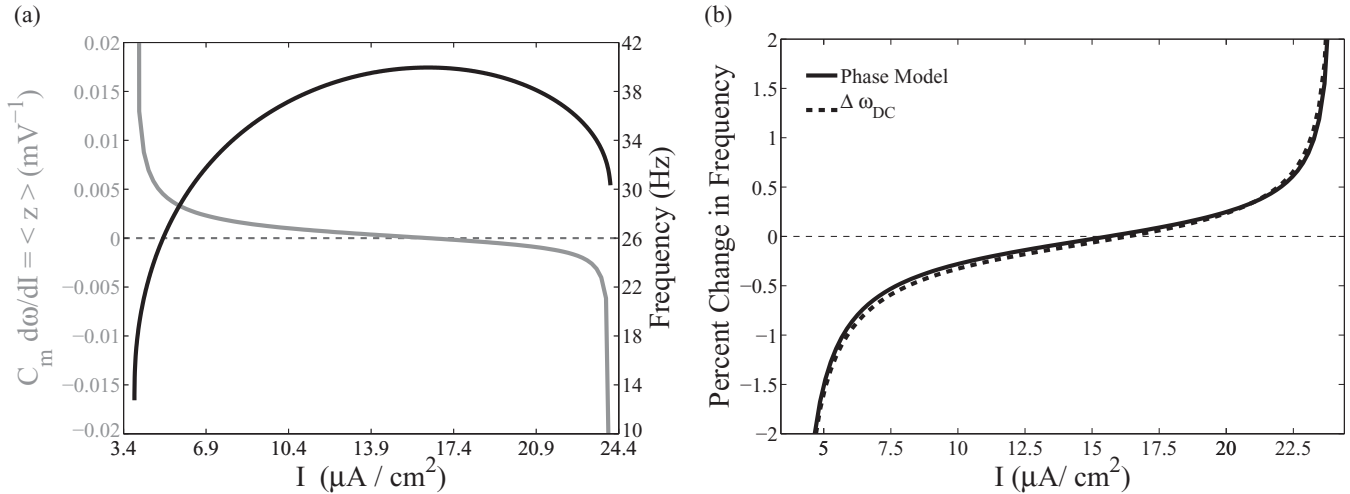


FIG. 6. (a) Frequency and average value of the somatic oscillator’s phase response curve  $\langle z \rangle$  vs  $I$ , for an isolated Morris-Lecar neuron. The plot of the gain of the neuron,  $\frac{d\omega}{dI}$ , is identical to that of  $\langle z \rangle / C_m$ . The point at which the frequency of the limit cycle oscillations (black curve) reaches a maximum occurs at the same point that  $\langle z \rangle$  (grey monotonically decreasing curve) reaches zero and subsequently becomes negative as  $I$  is increased. (b) Change in frequency caused by the presence of the dendrite,  $\Delta\omega$ , as a function of  $I$ . The solid line plots  $\Delta\omega$  and the dashed line plots  $\Delta\omega_{\text{DC}}$ . In this case, the dendrite is hyperpolarized ( $E_{LD} = -60$  mV) relative to the voltage oscillations, i.e.,  $\Delta I < 0$ . Thus, the dendritic load has a decelerating effect on frequency when  $\langle z \rangle > 0$  and an accelerating effect when  $\langle z \rangle < 0$ . Note that for these values of  $E_{LD}$  and  $\varepsilon(a)$ ,  $\Delta\omega_{\text{DC}}$  remains very close to  $\Delta\omega$ , and both  $\Delta\omega$  and  $\Delta\omega_{\text{DC}}$  retain the shape of the  $\langle z \rangle$  vs  $I$  curve.

hyperpolarizing dendritic load will lead to a decrease in firing frequency for relatively low applied currents, but there will be a “counterintuitive” increase in firing frequency for relatively high applied currents, as shown in Fig. 6(b).

## V. DISCUSSION

In this article, we examine how a passive dendritic load affects the firing frequency of a ball-and-stick model neuron. Using the theory of weak coupling, we derive an analytical expression that relates the change in frequency to the phase response properties of the model neuron and the properties of the dendrite [5]. We then elucidate the mechanisms that control the sensitivity of the neuron to dendritic load, and, in doing so, identify the mechanisms underlying the counterintuitive increases in firing frequency that can result from a hyperpolarizing dendritic load. Appendix D applies a similar analysis to an oscillator electrically coupled to a passive compartment, in which case very similar results are obtained.

Three main observations in this article allow the clear identification of the fundamental mechanisms underlying the changes in a neuron’s firing frequency caused by the addition of a dendritic load: (i) The dc component of the analytical expression for firing frequency,  $\Delta\omega_{\text{DC}}$ , typically dominates higher modes. This is the case unless the average of the PRC  $\langle z \rangle$  is tuned to be close to zero and/or the average of the oscillating membrane potential  $\langle v_{\text{LC}} \rangle$  is tuned to be close to the reversal potential of the dendrite  $E_{LD}$  (in these cases the change in frequency is very small). (ii) The form of  $\Delta\omega_{\text{DC}}$  indicates that the change in frequency caused by the dendritic load is primarily determined by the product  $\langle z \rangle \varepsilon(a) c_0(a) (E_{LD} - \langle v_{\text{LC}} \rangle)$ . Along with the observation (i), this implies that the effect of a passive dendritic load on a neuron’s firing frequency is equivalent to that of an additional constant current. The magnitude of this constant current is determined by the input conductance of the dendrite at the

soma normalized by somatic input conductance  $\varepsilon(a)c_0(a)$  and the average difference between the membrane potentials of the soma and dendrite  $E_{LD} - \langle v_{\text{LC}} \rangle$ . (iii) The average value of a PRC  $\langle z \rangle$  measures the sensitivity of the neuron to dendritic load and is proportional to the slope of the neuron’s  $f$ - $I$  curve. Thus, when  $\langle z \rangle > 0$  or equivalently  $\frac{df}{dI} > 0$ , the addition of a hyperpolarizing dendritic load causes the neuron’s frequency to decrease. When  $\langle z \rangle < 0$  or equivalently  $\frac{df}{dI} < 0$ , the addition of a hyperpolarizing dendritic load leads to a “counterintuitive” decrease in the firing frequency of a neuron. When  $\langle z \rangle \approx 0$  or equivalently  $\frac{df}{dI} \approx 0$ , the addition of a hyperpolarizing dendritic load causes a negligible change in firing frequency. Note that the failure of our intuition for this behavior arises from the preconception that frequency always increases with increased applied current.

The mechanisms discussed above provide a general framework for understanding the influence of passive dendritic properties on the firing frequency of neuronal oscillators. The numerical results presented in Sec. IV are for the Morris-Lecar model, but we have obtained similar results for several other neuronal models. For example, Fig. 7 shows that the dc component quantitatively captures the frequency modulation when somatic dynamics are described by the Traub *et al.* [19,20] model, which is a more biophysically detailed model (see Appendix B for equations). In fact,  $\langle z \rangle$  is relatively large over the entire oscillatory range for the Traub *et al.* model, and therefore the dc component correctly predicts the frequency modulation. On the other hand,  $\langle z \rangle$  is always positive, and therefore the counterintuitive increase in response to the addition of a hyperpolarizing dendritic load will not occur. A similar behavior would occur for any stereotypical “type-I” neuron [24].

Different neurons exhibit different  $f$ - $I$  curves under different conditions. Typically, the firing rate of a neuron increases with input strength, and often  $f$ - $I$  curves show saturation at high

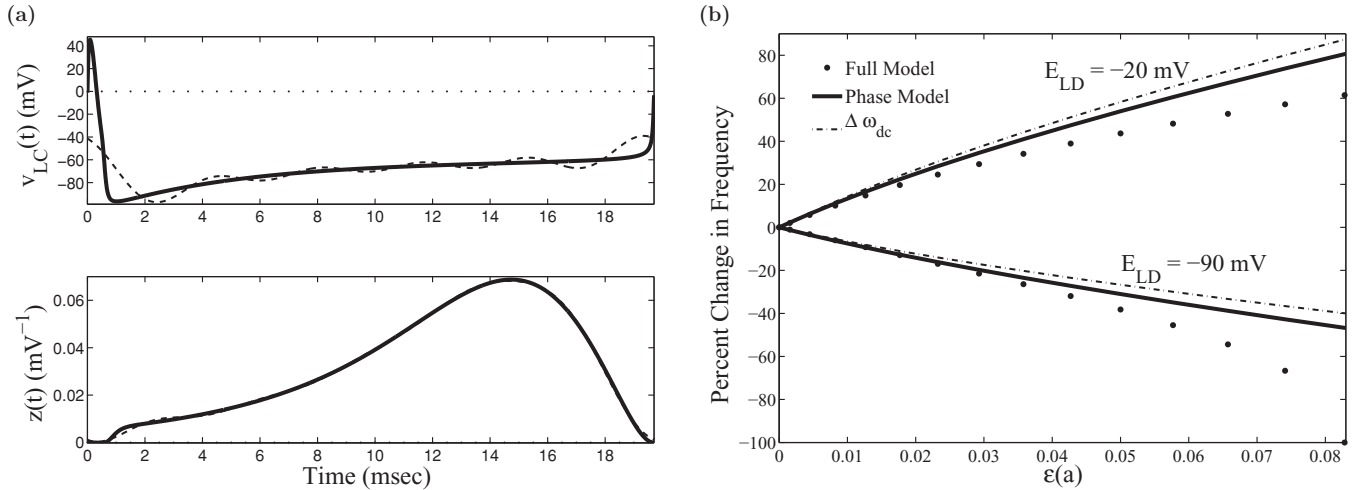


FIG. 7.  $\Delta\omega_{dc}$  dominates the behavior of the phase model for a more detailed model neuronal oscillator. (a) Voltage component of the limit cycle for the Traub *et al.* model neuron [20] when  $I = 1.2 \mu\text{A}/\text{cm}^2$  and its corresponding phase response curve. The dotted line in both plots is the approximation to the function using the first five Fourier modes.  $\langle v_{LC} \rangle = -68.02 \text{ mV}$  and  $\langle z \rangle = 0.032 \text{ mV}^{-1}$ . (b) The percent change in firing frequency is plotted as a function of the strength of the dendritic perturbation,  $\epsilon(a)$ , for a hyperpolarized ( $-90 \text{ mV}$ ) and depolarized ( $-20 \text{ mV}$ ) value of  $E_{LD}$  when  $I = 1.2 \mu\text{A}/\text{cm}^2$ . The dots represent results from simulations of the full ball-and-stick model [Eqs. (1)–(3)], the solid line represents results from simulations of the phase model [Eq. (15)], and the dashed-dotted line represents  $\Delta\omega_{dc}$  [Eq. (16)]. As in Fig. 2(a), the addition of the dendrite with a hyperpolarized leakage reversal potential decreases the frequency of oscillations as  $\epsilon(a)$  is increased while the addition of the dendrite with a depolarized leakage reversal potential increases the frequency of oscillations as  $\epsilon(a)$  is increased. It is important to note that  $\Delta\omega_{dc}$  remains close to the phase model for both values of the dendritic leakage reversal potential.

input levels. On the other hand, the firing rates of Hodgkin’s class 2 neurons [29] have little dependence on stimulus intensity. Furthermore, a nonmonotonic dependence of the firing rate on the strength of a constant applied current has also been observed in both models (e.g., Refs. [18,30,31]) and real neurons, including neurons in the lobster stomatogastric ganglion [30,31] and neocortical fast-spiking interneurons [32]. It has been shown that blocking or enhancing various ionic membrane conductances can promote saturation and nonmonotonicity in  $f$ - $I$  curves [21,30,31,33], and it has been recently demonstrated that noise can also promote saturation and nonmonotonicity [33].

Our results demonstrate that class 2 neurons and neurons operating near the saturation point of their  $f$ - $I$  curves have PRCs with near zero averages and are therefore insensitive to changes in dendritic load, which could be caused by neuromodulators or background synaptic input on the dendrites. Furthermore, the counterintuitive increase in frequency with a hyperpolarizing dendritic load that we have described can occur in neurons with nonmonotonic  $f$ - $I$  curves. In general, our results show that the frequency modulation caused by changes in the dendritic load can be quantified by the slope of the neuron’s  $f$ - $I$  curve.

Skinner *et al.* [31] found that cultured stomatogastric ganglion (STG) neurons can exhibit either monotonic or nonmonotonic  $f$ - $I$  curves and that neurons are able to switch between these two response properties with pharmacological manipulation. They demonstrated that modest changes of parameters can switch model neurons between these two behaviors. They also showed that, when model neurons with nonmonotonic  $f$ - $I$  curves are coupled by reciprocal inhibition, the frequency of the network can increase beyond the maximum frequency for an isolated cell. The mechanisms

responsible for this phenomena are intimately related to those described in this article

As mentioned before, the well-known modeling study by Kepler *et al.* [7] has previously examined the effects of electrically coupling a neuronal oscillator to a hyperpolarized passive cell in context of central pattern generators in the lobster STG. Kepler *et al.* found that, if the membrane potential of the neuronal oscillator has a short duty cycle [i.e., a predominantly hyperpolarized wave form as in Fig. 3(a)], the electrical load of the passive cell acts to decrease the frequency of oscillations as the strength of the electrical coupling is increased, whereas if the membrane potential of the neuron has a long duty cycle [i.e., a predominantly depolarized wave form as in Fig. 3(b)], the electrical load of the passive cell can increase the frequency of oscillations. Their explanation for this phenomenon was based on the balance of inward and outward currents in the oscillator compartment. More specifically, they postulated that, during the depolarized portion of the neuronal oscillations, the hyperpolarized passive compartment acts to more rapidly repolarize the neuronal oscillator and therefore acts to decrease the period of oscillation. On the other hand, during the subthreshold portion of the neuronal oscillations, the hyperpolarized passive compartment acts to slow the rate of depolarization toward threshold, and therefore it acts to increase the period of oscillation. When the neuronal oscillators have a short duty cycle, the cycle is dominated by the subthreshold phase and therefore the net effect of the passive load is to decrease the frequency of oscillations. Thus, if the neuronal oscillators have a long duty cycle, the cycle is dominated by the depolarized portion and the net effect of the passive load is to increase the frequency of oscillations.

Inherent in the explanation provided by Kepler *et al.* are the assumptions that the phase response curve of the oscillator will always be negative during the depolarized phase of the cycle and positive during the subthreshold phase of the cycle. Although this is the case for the simple model neuron that they used in their study, phase response properties of neuronal oscillators are typically more complicated than this (e.g., Fig. 3). For instance, neurons often have phase response curves with negative portions during the subthreshold phase [34]. The explanation provided in this article in terms of the oscillator's phase response curve is still conceptually simple and yet is more general than the explanation of Kepler *et al.* [7] in the sense that it can be applied to any oscillator.

In Appendix E, we consider the effects of constant and noisy point-source dendritic inputs on firing frequency. We show that constant point-source synaptic inputs to the thin dendrite are equivalent to shifting the value of the dendritic leakage reversal potential,  $E_{LD}$ . Furthermore, if the dendrite is subjected to white or exponentially correlated noisy input, the current that the soma receives will be a filtered version of the noise. The main effect of the noise on firing frequency is through its mean value. Because of the linearity of the cable, the mean of the noisy current would play the role of changing  $E_{LD}$  and shift the value of  $\Delta\omega$  in the phase model (15). Once the mean is accounted for, the situation falls into the framework considered by Teramae *et al.* [28], where a somatic oscillator is driven by filtered zero-mean white noise. The results of Teramae *et al.* [28] allow us to conclude that fluctuations in the noisy input will have negligible effects on firing frequency [28], and therefore the non-negligible effects must be through the mean of the noisy input.

The analysis presented in this paper relies on the assumption that the dendrites are thin relative to the diameter of the soma and therefore only weakly perturb the somatic dynamics. If the dendritic perturbation to a somatic oscillator is large, the dendritic load can fundamentally change the firing dynamics, e.g., quenching oscillations altogether, in which case our analysis may break down. On the other hand, our simulations show that the theory qualitatively predicts the firing effects of moderately sized dendritic perturbations despite the fact that the analysis takes the weak perturbation limit.

We have modeled the dendrite as a single cable, however, we expect that the addition of realistic dendritic morphologies will not substantially change our results. Many dendritic trees follow Rall's 3/2 rule, in which case they be described by an equivalent cylinder [35]. For these types of neurons, Van Ooyen *et al.* [36,37] directly showed that changes in dendritic topology have small effects on firing frequency. Furthermore, our analysis suggests that the key factors determining the dendrites' influence on the firing rate of a neuron are the input conductance of the dendritic tree at the soma-dendrite junction and the average membrane potential of the dendrites (encompassed by  $E_{LD}$ ). In fact, in their systematic study of the influence of the topology of dendritic tree on a neuron's firing rate, Van Ooyen *et al.* [37] concluded that most of the effects of a passive dendritic tree could be explained by the input conductance of the dendritic tree at the soma. Note that the input conductance of a passive dendritic tree can be analytically computed using an iterative method developed by Rall [35] or an alternative method developed by Van Pelt [38].

These observations suggest that our analysis holds if a portion of the proximal dendrite has a diameter that is sufficiently thin relative to the diameter to the soma.

Another assumption made in our analysis is that the dendrites are passive and do not contain active membrane conductances. Dendrites of some neurons contain highly active voltage-gated channels [39], and this would be expected to affect and perhaps fundamentally change the firing dynamics, e.g., inducing bursting dynamics [1,40]. However, recent evidence suggests that, in some neurons such as cerebellar stellate cells and hippocampal fast-spiking basket cells, dendrites express sodium channels at low density, if at all [41,42]. Therefore, the dendrites in these neurons should be well modeled by passive or weakly nonlinear cables. Our analysis can be readily extended to include weakly nonlinear and quasiactive conductances in the dendrites [43,44]. We note that we have found no fundamental changes in the results for this case. In fact, simulations by Van Ooyen *et al.* [37] showed that dependence of firing rate on dendritic topology were similar for dendritic trees with active and passive conductances. These observations suggest that the mechanisms underlying frequency modulation described here are applicable to a wide range of biologically relevant situations.

#### APPENDIX A: MORRIS-LECAR NEURON

$$C_m \frac{dv}{dt} = -g_{Ca} m_\infty[v(t)][v(t) - E_{Ca}] - g_K w \\ \times [v(t) - E_K] - g_L[v(t) - E_L] + I, \\ \frac{dw}{dt} = \phi \frac{w_\infty[v(t)] - w}{\tau_w[v(t)]},$$

where

$$m_\infty(v) = \frac{1}{2} \left[ 1 + \tanh \left( \frac{v - V_1}{V_2} \right) \right], \\ w_\infty(v) = \frac{1}{2} \left[ 1 + \tanh \left( \frac{v - V_3}{V_4} \right) \right], \\ \tau_w(v) = \frac{1}{\cosh \left( \frac{v - V_3}{2V_4} \right)},$$

and

$$C_m = 1 \mu\text{F}/\text{cm}^2, \quad g_{Ca} = 0.6 \text{ mS}/\text{cm}^2, \quad g_K = 0.8 \text{ mS}/\text{cm}^2 \\ g_L = 0.2 \text{ mS}/\text{cm}^2, \quad E_{Ca} = 100 \text{ mV}, \quad E_K = -80 \text{ mV}, \\ E_L = -50 \text{ mV}, \quad V_1 = 0 \text{ mV}, \quad V_2 = 15 \text{ mV}, \\ V_3 = 0 \text{ mV}, \quad V_4 = 15 \text{ mV}, \quad \phi = 0.08 \text{ ms}^{-1}.$$

The cable parameters with the Morris-Lecar neuron are

$$g_{LD} = 0.5 \text{ mS}/\text{cm}^2, \quad d = 0.002 \text{ cm}, \\ R_C = 0.1 \text{ k}\Omega \text{ cm}, \quad L = 0.02 \text{ cm}.$$

#### APPENDIX B: TRAUB MODEL SOMA

$$C_m \frac{dv}{dt} = -g_{Na} m^3 h[v(t) - E_{Na}] \\ - g_K n^4(v(t) - E_K) - g_L[v(t) - E_L] + I,$$

$$\begin{aligned}\frac{dm}{dt} &= \alpha_m(v)(1-m) - \beta_m(v)m, \\ \frac{dh}{dt} &= \alpha_h(v)(1-h) - \beta_h(v)h, \\ \frac{dn}{dt} &= \alpha_n(v)(1-n) - \beta_n(v)n,\end{aligned}$$

where

$$\begin{aligned}\alpha_m(v) &= 1.28 \frac{(v+54)/4}{1 - \exp[-(v+54)/4]}, \\ \beta_m(v) &= 1.4 \frac{(v+27)/5}{\exp[-(v+27)/5] - 1}, \\ \alpha_h(v) &= 0.128 \exp[-(v+50)/18], \\ \beta_h(v) &= 4.0 \frac{1}{1 + \exp[-(v+27)/5]}, \\ \alpha_n(v) &= 0.16 \frac{(v+52)/5}{1 - \exp[-(v+52)/5]}, \\ \beta_n(v) &= 0.5 \exp[-(v+57)/40],\end{aligned}$$

and

$$\begin{aligned}C_m &= 1 \mu\text{F}/\text{cm}^2, \quad g_{Na} = 100 \text{ mS}/\text{cm}^2, \\ g_K &= 80 \text{ mS}/\text{cm}^2, \quad g_L = 0.2 \text{ mS}/\text{cm}^2, \\ g_{LD} &= 0.5 \text{ mS}/\text{cm}^2, \quad E_{Na} = 50 \text{ mV}, \\ E_K &= -100 \text{ mV}, \quad E_L = -67 \text{ mV}.\end{aligned}$$

The cable parameters with the Traub model soma are

$$\begin{aligned}g_{LD} &= 0.5 \text{ mS}/\text{cm}^2, \quad d = 0.002 \text{ cm}, \\ R_C &= 0.1 \text{ k}\Omega \text{ cm}, \quad L = 0.01 \text{ cm}.\end{aligned}$$

### APPENDIX C: DENDRITIC EFFECTS IN THE BALL-AND-STICK PHASE MODEL

Recall that the “filtering” effects of the dendrite are captured by  $c_n(a)$  in Eq. (15). In this section, we show that the  $c_n(a)$  terms increase more slowly than the Fourier components  $v_n$  and  $z_n$  decay and that, for the parameters considered here,  $|c_n(a)| \approx 1$  for small  $n$ . Therefore, the higher-order cable properties of the dendrite (i.e., effects beyond the leakage reversal potential,  $E_{LD}$ ) do not greatly influence the behavior of the phase model for small  $n$ . Moreover, it is most often the case that the Fourier series of the phase response curve is dominated by the first few modes (see Figs. 3 and 7). Therefore, even if  $\varepsilon(a) \frac{\partial V}{\partial x}(0, t)$  contains higher modes in its Fourier expansion, they will be “zeroed out” when multiplied by the PRC. Thus, the phase model will not be greatly influenced by the cable properties and will be dominated by the first few modes of the Fourier expansion of the  $\Delta\omega$  term.

Recall that  $c_n(a) = b_n \tanh[b_n \frac{L}{\lambda(a)}]$ , with  $b_n = \sqrt{1 + \frac{g_L}{g_{LD}} 2\pi i n / \bar{T}}$ . For a sufficiently long dendrite  $\frac{L}{\lambda(a)} \geq 1.5$ ,  $|\tanh(b_n \frac{L}{\lambda(a)})| \in [0.9, 1.3]$ . Thus,  $c_n(a) \approx b_n$ . Using the fact that the nondimensional period,  $\bar{T}$ , is equal to the dimensional

period,  $T$ , divided by the somatic membrane time constant,  $\tau_S$ , and the fact that  $\tau_D = \frac{C_m}{g_{LD}}$ , we can rewrite  $c_n(a)$  as

$$c_n(a) \approx b_n = \sqrt{1 + \frac{\tau_D}{\tau_S} 2\pi i n \frac{\tau_S}{T}} = \sqrt{1 + \frac{\tau_D}{T} 2\pi i n}. \quad (\text{C1})$$

The magnitude and angle of the  $c_n(a)$  terms is then given by

$$|c_n(a)| = \left[ 1 + n^2 \left( \frac{\tau_D}{T} 2\pi \right)^2 \right]^{1/4}, \quad (\text{C2})$$

$$\phi_n = \frac{1}{2} \arctan \left( 2\pi n \frac{\tau_D}{T} \right). \quad (\text{C3})$$

Thus,  $|c_n(a)|$  increases as  $n^{1/2}$ . This implies that the effect of dendrite acts to amplify the higher modes in the Fourier series. However, if  $\frac{\tau_D}{T} \ll 1$ , then  $|c_n(a)| \approx 1$  for small  $n$ .

For our simulations, the dendritic membrane time constant,  $\tau_D$ , is set at 2 ms, and the space constant,  $\lambda(a)$ , ranges from  $O(10^{-3})$  to  $O(10^{-2})$  cm for the values of dendritic radii that were used. For the Morris-Lecar and Traub *et al.* model neurons,  $\frac{\tau_D}{T} \sim O(10^{-1})$ . Thus, because the Fourier coefficients  $z_n$  rapidly decay and  $|c_n(a)| \approx 1$  for small  $n$ , the higher-order cable properties have a minimal effect on the phase model.

### APPENDIX D: TWO-COMPARTMENT MODEL

In this section we present the phase model reduction for the two-compartment model of a soma electrically coupled to a dendritic compartment. In this case, the phase model can be obtained using two different limits: the limit of weak electrical coupling and the limit of a large oscillator compartment attached to a smaller dendritic compartment. However, in both limits, the behavior of the phase model qualitatively matches that of the phase model derived from the ball-and-stick model. Thus, our explanation for the non-intuitive frequency effects seen in the cable model can be directly applied to the two-compartment model studied in Kepler *et al.* [7].

The soma is modeled as an isopotential compartment with Hodgkin-Huxley currents and the dendrite is modeled as a passive compartment electrically coupled to the soma [6],

$$C_m \frac{dv_S}{dt} = -I_{\text{ion},S}[v_S(t), \vec{w}] + I + g_C \left( \frac{a_D}{a_S} \right)^2 (v_D - v_S), \quad (\text{D1})$$

$$C_m \frac{dv_D}{dt} = -g_{LD}(v_D - E_{LD}) + g_C(v_S - v_D), \quad (\text{D2})$$

where  $v_S(t)$  and  $v_D(t)$  represent the voltage, in mV, of the somatic and dendritic compartment, respectively, at time  $t$ ,  $g_C$  is the gap junctional conductance in  $\text{mS}/\text{cm}^2$ ,  $a_S$  and  $a_D$  represent the radii of the somatic and dendritic compartments, respectively, in cm, and  $I_{\text{ion},S}(v, \vec{w})$ ,  $\bar{I}$ ,  $g_{LD}$ ,  $C_m$ , and  $E_{LD}$  are the same as in the ball-and-stick model. In addition,  $I$  is assumed to be large enough so that the soma undergoes periodic firing, i.e., limit cycle oscillations.

Let  $V_{S,D} = V_{S,D}(t) = \frac{v_{S,D}(\tau_D \bar{t}) - E_L}{-E_L}$  (where  $E_L$  is the leakage reversal potential in the soma),  $\bar{t} = \frac{t}{\tau_D}$ , and  $\tau_D = C_m/g_{LD}$  is the membrane time constant of the dendritic compartment.

Then, our equations become

$$\frac{dV_S}{d\bar{t}} = -\bar{I}_{\text{ion},S}[V(\bar{t}), \bar{w}] + \bar{I} + \varepsilon\gamma(V_D - V_S), \quad (\text{D3})$$

$$\frac{dV_D}{d\bar{t}} = -(V_D - \bar{E}_{LD}) + \varepsilon(V_S - V_D), \quad (\text{D4})$$

where  $\gamma = (\frac{a_D}{a_S})^2$ ,  $\varepsilon = \frac{g_C}{g_{LD}}$ , and  $\bar{E}_{LD}$ ,  $\bar{I}_{\text{ion},S}[V(\bar{t}), \bar{w}]$ , and  $\bar{I}$  are the same as for the ball-and-stick model.

There are two possible approaches to the phase reduction at this point: (1) Assume that  $\varepsilon$  is the small parameter, or (2) assume that  $\gamma$  is the small parameter. Let us first examine the case where  $\varepsilon$  is small and  $\gamma$  is  $O(1)$ .

As with the ball-and-stick model, we can reduce the dynamics of our two-compartment model to a single-phase equation by assuming that  $g_C \ll g_{LD}$  and that  $\gamma$  is  $O(1)$ . Note, in this case, our assumption is that the coupling between the two compartments is what we are assuming is small while the ratio of the radii is assumed to be  $O(1)$ . Because  $\varepsilon$  appears in both Eqs. (D3) and (D4), both compartments will be behaving very similarly to their unperturbed ( $\varepsilon = 0$ ) counterparts. Thus, the dendritic compartment will go to its steady state,  $\bar{E}_{LD}$ , and the membrane potential of the somatic compartment will go to its limit cycle,  $V_{LC}(\bar{t})$ . Our phase equation is then

$$\frac{d\theta}{d\bar{t}} = \bar{\omega} + \Delta\bar{\omega} = \bar{\omega} + \frac{\varepsilon\gamma}{\bar{T}} \int_0^{\bar{T}} Z(s)[\bar{E}_{LD} - V_{LC}(s)] ds, \quad (\text{D5})$$

where  $\varepsilon\gamma(\bar{E}_{LD} - V_{LC})$  is the nondimensional coupling current under the assumption that both  $V_S$  and  $V_D$  cling tightly to their steady states. Expanding  $Z(\bar{t})$  and  $V_{LC}(\bar{t})$  in a Fourier series yields

$$\frac{d\theta}{d\bar{t}} = \bar{\omega} + \varepsilon\gamma\langle Z \rangle(\bar{E}_{LD} - \langle V_{LC} \rangle) - \frac{\varepsilon\gamma}{\bar{T}^2} \sum_{n \neq 0} Z_{-n} V_n. \quad (\text{D6})$$

where  $V_n$  are the coefficients of  $V_{LC}$ ,  $Z_n$  are the coefficients of  $Z$ , and we have replaced  $V_0/\bar{T}$  and  $Z_0/\bar{T}$  with  $\langle V_{LC} \rangle$ , and  $\langle Z \rangle$  as in Eq. (15). Note that this is the same as the phase equation for the ball-and-stick model without the terms describing the influence of the cable, i.e.,  $c_n(a)$ .

Next, let us assume that  $\gamma$  is small and that  $\varepsilon$  is  $O(1)$ . In this case, we are assuming that the somatic compartment is much larger than the dendritic compartment. Thus, the dendrite will have a minimal effect on the dynamics of the soma, implying that the membrane potential of the somatic compartment will cling to its limit cycle,  $V_{LC}(\bar{t})$ , while the somatic compartment will have an  $O(1)$  effect on the dynamics of the dendritic compartment. Our phase equation is then

$$\frac{d\theta}{d\bar{t}} = \bar{\omega} + \Delta\bar{\omega} = \bar{\omega} + \frac{\varepsilon\gamma}{\bar{T}} \int_0^{\bar{T}} Z(s)[V_D(s) - V_{LC}(s)] ds, \quad (\text{D7})$$

where the first order approximation to  $V_D(\bar{t})$  is found by solving

$$\frac{dV_D}{d\bar{t}} = -(V_D - \bar{E}_{LD}) + \varepsilon[V_{LC}(\bar{t}) - V_D]. \quad (\text{D8})$$

Solving the above equation using a Fourier series and plugging the result into Eq. (D7) yields

$$\frac{d\theta}{d\bar{t}} = \bar{\omega} + \gamma\langle Z \rangle(\bar{E}_{LD} - \langle V_{LC} \rangle) \left( \frac{\varepsilon}{1 + \varepsilon} \right) - \frac{\gamma}{\bar{T}^2} \sum_{n \neq 0} Z_{-n} V_n c_n, \quad (\text{D9})$$

where  $c_n = \frac{\varepsilon(1+2\pi in/\bar{T})}{2\pi in/\bar{T} + (1+\varepsilon)}$ . Thus, in this limit, there are filtering effects owing to the addition of the dendritic compartment. Recall that time was nondimensionalized using  $\tau_D$ . This implies that  $\bar{T} = T/\tau_D$ , where  $T$  is the dimensional period of oscillations. Therefore, the magnitude of the  $c_n$  terms can be written as

$$|c_n| = \varepsilon \left[ \frac{1 + (2\pi n \frac{\tau_D}{\bar{T}})^2}{(2\pi n \frac{\tau_D}{\bar{T}})^2 + (1 + \varepsilon)^2} \right]^{1/2}. \quad (\text{D10})$$

Equation (D10) limits to 1 as  $n \rightarrow \infty$ . When  $\frac{\tau_D}{\bar{T}} \ll 1$ ,  $|c_n| \approx \frac{\varepsilon}{1+\varepsilon}$  for small  $n$ , which implies that the filtering effects are minimal.

In both scenarios presented above, the phase models qualitatively match the dynamics of the phase model derived from the ball-and-stick model.

#### APPENDIX E: THE EFFECTS OF DENDRITIC INPUTS AT POINT SOURCES

In this section, we discuss how inputs to a thin dendrite affect the frequency of the somatic oscillator. We show that point-source inputs to the thin dendrite have the same effect on the frequency as shifting the leakage reversal potential of the dendrite,  $E_{LD}$ , by a constant value.

In the limit of  $\varepsilon \ll 1$ , a dendrite receiving  $K$  point-source inputs and being driven by an oscillatory soma is described by the following system of equations:

$$g \frac{\partial V}{\partial \bar{t}} = \frac{\partial^2 V}{\partial \bar{x}^2} - (V - \bar{E}_{LD}) + \sum_{n=1}^K \bar{A}_n \delta(\bar{x} - \bar{x}_n), \quad (\text{E1})$$

$$V(0, \bar{t}) = V_{LC}(\bar{t}), \quad (\text{E2})$$

$$\frac{\partial V}{\partial \bar{x}} \left[ \frac{L}{\lambda(a)}, \bar{t} \right] = 0. \quad (\text{E3})$$

Using the principle of superposition, we can separate out the dendritic inputs and the oscillatory boundary condition and solve

$$g \frac{\partial V}{\partial \bar{t}} = \frac{\partial^2 V}{\partial \bar{x}^2} - V + \sum_{n=1}^K \bar{A}_n \delta(\bar{x} - \bar{x}_n), \quad (\text{E4})$$

$$V(0, \bar{t}) = 0, \quad (\text{E5})$$

$$\frac{\partial V}{\partial \bar{x}} \left[ \frac{L}{\lambda(a)}, \bar{t} \right] = 0, \quad (\text{E6})$$

and

$$g \frac{\partial V}{\partial \bar{t}} = \frac{\partial^2 V}{\partial \bar{x}^2} - (V - \bar{E}_{LD}), \quad (\text{E7})$$

$$V(0, \bar{t}) = V_{LC}(\bar{t}), \quad (\text{E8})$$

$$\frac{\partial V}{\partial \bar{x}} \left[ \frac{L}{\lambda(a)}, \bar{t} \right] = 0, \quad (\text{E9})$$

separately. Note that we solve Eqs. (E7)–(E9) in Sec. III. Because we are concerned with the steady-state current that the dendritic inputs cause to be injected into the soma, we can set the time derivative equal to zero in (E4) and solve

$$-\frac{d^2V}{d\bar{x}^2} + V = \sum_{n=1}^K \bar{A}_n \delta(\bar{x} - \bar{x}_n), \quad (\text{E10})$$

$$g(\bar{x}, \bar{x}_n) = \begin{cases} \bar{A}_n \sinh(\bar{x}) \cosh[\bar{x}_n - \frac{L}{\lambda(a)}] / \cosh[\frac{L}{\lambda(a)}] & \text{if } 0 \leq \bar{x} \leq \bar{x}_n \leq \frac{L}{\lambda(a)}, \\ \bar{A}_n \sinh(\bar{x}_n) \cosh[\bar{x} - \frac{L}{\lambda(a)}] / \cosh[\frac{L}{\lambda(a)}] & \text{if } 0 \leq \bar{x}_n \leq \bar{x} \leq \frac{L}{\lambda(a)}. \end{cases} \quad (\text{E13})$$

Therefore, the current that the soma receives from these  $K$  dendritic inputs is given by the following constant term:

$$\bar{I}_{\text{input}} = \sum_{n=1}^K g_{\bar{x}}(0, \bar{x}_n) = \sum_{n=1}^K \bar{A}_n \frac{\cosh[\bar{x}_n - \frac{L}{\lambda(a)}]}{\cosh[\frac{L}{\lambda(a)}]}. \quad (\text{E14})$$

Adding the above term to Eq. (13) yields

$$\begin{aligned} \frac{\partial V}{\partial \bar{x}}(0, \bar{t}) \\ = \left( \bar{E}_{LD} - \frac{V_0}{\bar{T}} \right) c_0(a) - \frac{1}{\bar{T}} \sum_{n \neq 0} c_n(a) V_n e^{2\pi i n \bar{t} / \bar{T}} + \bar{I}_{\text{input}}. \end{aligned} \quad (\text{E15})$$

This changes the phase equation (15) to

$$\begin{aligned} \frac{d\theta}{dt} = \omega + \frac{\varepsilon(a)}{\tau_S} \left\{ \langle z \rangle \left[ (E_{LD} - \langle v_{LC} \rangle) c_0(a) + \frac{1}{g_{LD}} I_{\text{input}} \right] \right. \\ \left. - \frac{2}{\bar{T}^2} \sum_{n=1}^{\infty} |z_n v_n c_n(a)| \cos[\psi_n(a) + \gamma_n - \phi_n] \right\}, \end{aligned} \quad (\text{E16})$$

where  $I_{\text{input}} = -g_{LD} E_L \bar{I}_{\text{input}}$ . Thus, the addition of point-source inputs to the dendrite can be completely incorporated into  $E_{LD}$ , as  $c_0(a) \sim 1$  for the parameter range we considered.

The above argument can be extended to include noisy point-source inputs to the dendrite. Teramae *et al.* [28] show that, for filtered zero-mean noisy input of amplitude  $O(\sigma)$  injected

$$V(0) = 0, \quad (\text{E11})$$

$$\frac{dV}{d\bar{x}} \left[ \frac{L}{\lambda(a)} \right] = 0. \quad (\text{E12})$$

The solution of the above system is given by the following Green's function:

directly into a somatic oscillator, the filtered noise had  $O(\sigma^2)$  effects on the mean frequency of the oscillator. The  $O(\sigma^2)$  terms involve the correlation time of the colored noise, the relaxation time back to the limit cycle, and higher-order phase response properties of the somatic limit cycle. If the correlation time of the noisy input is comparable to the relaxation time back to the somatic limit cycle, then the effects of the noisy input on firing frequency cannot be ignored. These effects are difficult to obtain computationally as they involve higher-order phase response properties of the limit cycle [28,45]. On the other hand, if the correlation time of the noise is larger than the relaxation time back to the somatic limit cycle, then fluctuations in the noisy input will have negligible effects on firing frequency [28].

The situation of noisy inputs to the dendrite can be covered under the framework of Teramae *et al.* [28] as the noisy input that reaches the soma will be a filtered version of the noisy input at the dendrite. However, in our case, the amplitude of the noisy input can be large as long as the current at the dendro-somatic junction remains  $O(\varepsilon)$ . Furthermore, the filtering properties of the dendrite act to increase the correlation time of the noise. Thus, our situation corresponds to the case in Teramae *et al.*, where the correlation time of the noise is larger than the relaxation time back to the limit cycle, which implies that fluctuations in the noisy input have negligible effects on the mean firing frequency of the somatic oscillator. However, the mean of the noisy input can still have an  $O(\varepsilon)$  on the mean firing frequency as discussed above.

- 
- [1] Z. Mainen and T. Sejnowski, *Nature (London)* **382**, 363 (1996).  
 [2] C. Koch and I. Segev, *Nat. Neurosci.* **3**, 1171 (2000).  
 [3] P. Lánský and R. Rodríguez, *Biol. Cybern.* **81**, 161 (1999).  
 [4] P. C. Bressloff and S. Coombes, *Phys. Rev. Lett.* **78**, 4665 (1997).  
 [5] S. Crook, G. Ermentrout, and J. Bower, *J. Comput. Neurosci.* **5**, 315 (1998).  
 [6] T. Lewis and J. Rinzel, *Neurocomputing* **58-60**, 145 (2004).  
 [7] T. Kepler, E. Marder, and L. Abbott, *Science* **248**, 83 (1990).  
 [8] A. A. Sharp, L. F. Abbott, and E. Marder, *J. Neurophysiol.* **67**, 1691 (1992).  
 [9] M. Dolnik, T. S. Gardner, I. R. Epstein, and J. J. Collins, *Phys. Rev. Lett.* **82**, 1582 (1999).  
 [10] W. Rall, *Exp. Neurol.* **2**, 503 (1960).  
 [11] J. Neu, *SIAM J. Appl. Math.* **37**, 307 (1979).  
 [12] G. Ermentrout, *J. Math. Biol.* **12**, 327 (1981).  
 [13] Y. Kuramoto, *Chemical Oscillations, Waves, and Turbulence* (Springer-Verlag, Berlin, 1984).  
 [14] W. Rall, *Science* **126**, 454 (1957).  
 [15] W. Rall, *Biophys. J.* **9**, 1483 (1969).  
 [16] A.-L. Hodgkin and A. F. Huxley, *J. Physiol. (London)* **117**, 500 (1952).  
 [17] C. Morris and H. Lecar, *Biophys. J.* **35**, 193 (1981).  
 [18] J. Rinzel and G. Ermentrout, in *Methods in Neuronal Modeling: From Synapses to Networks*, edited by C. Koch and I. Segev (MIT Press, Cambridge, MA, 1989), pp. 135–171.  
 [19] F. C. Hoppensteadt and C. S. Peskin, *Modeling and Simulation in Medicine and the Life Sciences. Second Edition* (Springer-Verlag, New York, 2002).

- [20] R. Traub and R. Miles, *J. Comput. Neurosci.* **2**, 291 (1995).
- [21] A. Erisir, D. Lau, B. Rudy, and C. S. Leonard, *J. Neurophysiol.* **82**, 2476 (1999).
- [22] R. FitzHugh, *Biophys. J.* **1**, 445 (1961).
- [23] L. Abbott, *Brain Res. Bull.* **50**, 303 (1999).
- [24] G. Ermentrout, *Neural Comput.* **8**, 1979 (1996).
- [25] F. C. Hoppensteadt and E. M. Izhikevich, *Weakly Connected Neural Networks* (Springer-Verlag, New York, 1997).
- [26] B. Pfeuty, G. Mato, D. Golomb, and D. Hansel, *J. Neurosci.* **23**, 6280 (2003).
- [27] T. Lewis and J. Rinzel, *J. Comput. Neurosci.* **14**, 283 (2003).
- [28] J. N. Teramae, H. Nakao, and G. B. Ermentrout, *Phys. Rev. Lett.* **102**, 194102 (2009).
- [29] A. L. Hodgkin, *J. Physiol. (London)* **107**, 165 (1948).
- [30] K. Szaliszynó, *J. Comput. Neurosci.* **20**, 137 (2006).
- [31] F. K. Skinner, G. G. Turrigiano, and E. Marder, *Biol. Cybern.* **69**, 375 (1993).
- [32] T. Tateno, A. Harsch, and H. Robinson, *J. Neurophysiol.* **92**, 2283 (2004).
- [33] B. Lundstrom, M. Famulare, L. Sorensen, W. Spain, and A. Fairhall, *J. Comput. Neurosci.* **27**, 277 (2009).
- [34] J. Mancilla, T. Lewis, D. Pinto, J. Rinzel, and B. Connors, *J. Neurosci.* **27**, 2058 (2007).
- [35] W. Rall, *Exp. Neurol.* **2**, 491 (1959).
- [36] J. Duijnhouwer, M. Remme, A. van Ooyen, and J. van Pelt, *Neurocomputing* **38–40**, 183 (2001).
- [37] A. van Ooyen, J. Duijnhouwer, M. W. Remme, and J. van Pelt, *Network: Comput. Neural Syst.* **13**, 311 (2002).
- [38] J. Van Pelt, *Biol. Cybern.* **68**, 15 (1992).
- [39] D. Johnston and R. Narayanan, *Trends Neurosci.* **31**, 309 (2008).
- [40] A. Bose and V. Booth, in *Bursting: The Genesis of Rhythm in the Nervous System*, edited by S. Coombes and P. Bressloff (World Scientific, Singapore, 2005), pp. 123–144.
- [41] H. Hu, M. Martina, and P. Jonas, *Science* **327**, 52 (2009).
- [42] M. Myoga, M. Beierlein, and W. Regehr, *J. Neurosci.* **29**, 7803 (2009).
- [43] J. A. Goldberg, C. A. Deister, and C. J. Wilson, *J. Neurophysiol.* **97**, 208 (2007).
- [44] P. C. Bressloff, *J. Comput. Neurosci.* **6**, 237 (1999).
- [45] K. Yoshimura and K. Arai, *Phys. Rev. Lett.* **101**, 154101 (2008).